

## Pathways for proton release during ubihydroquinone oxidation by the $bc_1$ complex

ANTONY R. CROFTS\*<sup>†‡§</sup>, SANGJIN HONG<sup>‡</sup>, NATALIA UGULAVA<sup>‡</sup>, BLANCA BARQUERA\*, ROBERT GENNIS\*<sup>‡</sup>,  
MARIANA GUERGOVA-KURAS<sup>‡</sup>, AND EDWARD A. BERRY<sup>¶</sup>

Departments of \*Biochemistry and <sup>†</sup>Microbiology and <sup>‡</sup>Center for Biophysics and Computational Biology, University of Illinois at Urbana–Champaign, Urbana, IL 61801; and <sup>¶</sup>Lawrence Berkeley National Laboratory, University of California, Berkeley, CA 94720

Edited by Pierre A. Joliot, Institute of Physico-Chemical Biology, Paris, France, and approved July 6, 1999 (received for review May 5, 1999)

**ABSTRACT** Quinol oxidation by the  $bc_1$  complex of *Rhodobacter sphaeroides* occurs from an enzyme–substrate complex formed between quinol bound at the  $Q_o$  site and the iron–sulfur protein (ISP) docked at an interface on cytochrome  $b$ . From the structure of the stigmatellin-containing mitochondrial complex, we suggest that hydrogen bonds to the two quinol hydroxyl groups, from Glu-272 of cytochrome  $b$  and His-161 of the ISP, help to stabilize the enzyme–substrate complex and aid proton release. Reduction of the oxidized ISP involves H transfer from quinol. Release of the proton occurs when the acceptor chain reoxidizes the reduced ISP, after domain movement to an interface on cytochrome  $c_1$ . Effects of mutations to the ISP that change the redox potential and/or the pK on the oxidized form support this mechanism. Structures for the complex in the presence of inhibitors show two different orientations of Glu-272. In stigmatellin-containing crystals, the side chain points into the site, to hydrogen bond with a ring hydroxyl, while His-161 hydrogen bonds to the carbonyl group. In the native structure, or crystals containing myxothiazol or  $\beta$ -methoxyacrylate-type inhibitors, the Glu-272 side chain is rotated to point out of the site, to the surface of an external aqueous channel. Effects of mutation at this residue suggest that this group is involved in ligation of stigmatellin and quinol, but not quinone, and that the carboxylate function is essential for rapid turnover.  $H^+$  transfer from semiquinone to the carboxylate side chain and rotation to the position found in the myxothiazol structure provide a pathway for release of the second proton.

The  $bc_1$  complex family of enzymes plays a central role in all the main pathways of energy conversion, and the photosynthetic apparatus of *Rhodobacter sphaeroides* exemplifies one of the simplest of these (1–5). This system is convenient experimentally because of the ease with which electron transfer can be initiated by illumination (6). X-ray crystallographic structures of mitochondrial complexes (7–10) contain at their core the three catalytic subunits, cytochrome (cyt)  $b$ , cyt  $c_1$ , and the Rieske iron–sulfur protein (ISP), common to the bacterial enzymes (11–13). Homology models of these show that the catalytic superstructure is highly conserved, as had been expected from studies of the mechanism, which is essentially the same in the two systems (1–5). The  $bc_1$  complex catalyzes the oxidation of quinol and the reduction of cyt  $c$  (or  $c_2$ ) through a modified Q cycle (1–6, 14–17). Two separate internal electron transfer chains connect three catalytic sites. At one site, heme  $c_1$  is oxidized by cyt  $c_2$ . Two catalytic sites in cyt  $b$  are involved in oxidation or reduction of ubiquinone. In the bifurcated reaction at the quinol-oxidizing site (the  $Q_o$  site), one electron from quinol is passed to the ISP, which transfers it to cyt  $c_1$ , while the semiquinone produced is

oxidized by another chain consisting of the two  $b$  hemes of cyt  $b$ . At the quinone-reducing site ( $Q_i$ -site), electrons from the  $b$ -heme chain are used to generate quinol. The integration of the oxidation and reduction reactions with the release or uptake of protons in the aqueous phases allows the complex to pump protons across the membrane.

The reaction at the  $Q_o$  site determines the unique functional characteristics of the  $bc_1$  complex. The bifurcation of electrons between high- and low-potential chains is the crucial event through which the free-energy drop between the quinol pool and oxidized acceptor is used to generate a proton gradient. The efficiency of this process is therefore of primary importance in energy conversion. The complex has evolved to maximize the efficiency, and it achieves a remarkable partitioning in which the second electron is passed almost exclusively to the low-potential heme  $b_L$ , despite the more favorable redox gradient provided by the high-potential chain  $b_H$ .

In this paper, we identify the pathways by which protons are released from the  $Q_o$  site on quinol oxidation. The mechanism we propose is based on an analysis of the binding of inhibitors at the  $Q_o$  site as shown by the structures, and on the pH dependence of activation barriers in the partial reactions of the site, of turnover, and of the redox properties of the centers. Our mechanism accounts for the functional modifications on mutation of a highly conserved glutamate of the -PEWY- loop (named from the sequence in single-letter code) of cyt  $b$ , and of residues of the ISP that lead to changes in redox potential and pK, which previously had seemed paradoxical.

### EXPERIMENTAL PROCEDURES

Structures of the complex from chicken heart mitochondria have been discussed elsewhere (8). Refined structures have also been solved at similar resolution for the chicken complexes with myxothiazol or  $\beta$ -methoxyacrylate (MOA)-stilbene bound. Refinement data for deposited structures (1bcc, 2bcc, and 3bcc) are included in the files, and data for other structures are similar and will be published elsewhere.

This paper was submitted directly (Track II) to the *Proceedings* office. Abbreviations:  $bc_1$  complex, ubihydroquinone:cytochrome  $c$  oxidoreductase (EC 1.10.2.2);  $b_L$  and  $b_H$ , low-potential and higher-potential hemes of cytochrome  $b$ ; cyt, cytochrome; ISP, Rieske-type iron–sulfur protein; ISP<sub>ox</sub> and ISP<sub>red</sub>, oxidized and reduced forms of the ISP; MOA-stilbene, substituted stilbene with  $\beta$ -methoxyacrylate as the pharmacologically active group; Q, quinone form of ubiquinone-10; QH<sub>2</sub>, hydroquinone, or quinol, form of ubiquinone-10;  $Q_i$  site, quinone-reducing site of the  $bc_1$  complex;  $Q_o$  site, hydroquinone-oxidizing site of the  $bc_1$  complex.

Data deposition: The atomic coordinates for the chicken mitochondrial  $bc_1$  complex have been deposited in the Protein Data Bank, www.rcsb.org (PDB ID codes: native, 1bcc; with stigmatellin, 2bcc; with stigmatellin and antimycin, 3bcc).

<sup>§</sup>To whom reprint requests should be addressed at: Center for Biophysics and Computational Biology, University of Illinois at Urbana–Champaign, 388 Morrill Hall, 505 South Goodwin, Urbana, IL 61801. E-mail: a-crofts@uiuc.edu.

The publication costs of this article were defrayed in part by page charge payment. This article must therefore be hereby marked “advertisement” in accordance with 18 U.S.C. §1734 solely to indicate this fact.

PNAS is available online at www.pnas.org.

Modeling of the quinones at the  $Q_o$  site was performed with SCULPT (18) (Interactive Simulations, acquired by MDL Information Systems, San Leandro, CA) running on a PC computer. After removal of the coordinate data for the incumbent inhibitor, the quinone abstracted from PDB file 4rcr (photochemical reaction center) was positioned at the  $Q_o$  site to mimic the inhibitor. To model the occupancy of the distal domain, the stigmatellin-containing structure was used. For occupancy of the proximal domain, the myxothiazol structure was used. After preliminary manipulation, the quinone was allowed to relax with the protein frozen to force conformation to the site volume. In the distal position, the quinone head was constrained by tethering the two carbonyl O atoms, one to  $N^\epsilon$  of His-161 and one to  $O^\epsilon 1$  of Glu-272. This tethered relaxation resulted in distances suitable for H bonds, which were represented by adding H atoms to mimic the ligation of the quinol. Water molecules in the putative water chain were based on a model constructed for molecular dynamics simulation (39), with some relaxation to accommodate residue changes in different structures.

Kinetic measurements and determination of activation energies were essentially as described previously (17). Measurement of redox potentials for cytochromes (15, 16) and the ISP (19) were as described in the references. Mutagenesis was performed essentially as described in ref. 20, and measurements of EPR spectra of the ISP were as described in ref. 21. Details of mutagenic primers will be described elsewhere.

## RESULTS

**Inhibitor and Substrate Complexes at the  $Q_o$  Site.** The binding of stigmatellin at the  $Q_o$  site is shown in Fig. 1 *Upper*.

The model is based on the chicken mitochondrial complex with stigmatellin (PDB ID 2bcc), and further refinement of the crystals containing stigmatellin and antimycin previously described (ref. 8, deposited as 3bcc). The  $Q_o$  site has a bifurcated volume, with lobes distal from and proximal to heme  $b_L$ . The inhibitor is constrained at the distal end of the binding pocket, as previously observed, through its interaction with the ISP. However, in the revised configuration, stigmatellin is rotated by  $180^\circ$  compared with that in 3bcc (8). The inhibitor is liganded by a bond between His-161 of the ISP and the carbonyl O atom of the chromone ring. His-161 is also a ligand to the 2Fe–2S cluster and has been identified as the group responsible for the  $pK$  of  $\approx 7.6$  on the oxidized ISP (ISP<sub>ox</sub>) (22, 23). In contrast to published structures (7–9), a second ligand to stigmatellin has now been identified, provided by Glu-272 of the highly conserved -PEWY- loop. The carboxylate of the side chain of Glu-272 is found within H-bonding distance of the -OH group of the second ring of stigmatellin, diagonally across from the carbonyl group. To bind to the inhibitor, the side chain has rotated from the position in the absence of inhibitor, where it points out of the site. The side chain is also found in the “out” position when myxothiazol or MOA-stilbene binds at the site, and rotation out of the binding domain is necessary to accommodate these inhibitors. In the “out” position, the carboxylate group forms part of the exterior-facing surface of a cavity reaching into the protein from the aqueous phase on the P side of the structure.

Lancaster and Michel (24) have suggested that in reaction centers, stigmatellin might mimic an intermediate of the reaction cycle—either the neutral semiquinone or the quinol anion,  $QH^-$ . Link (25) has proposed that in the  $bc_1$  complex, stigmatellin mimics a complex between semiquinone and

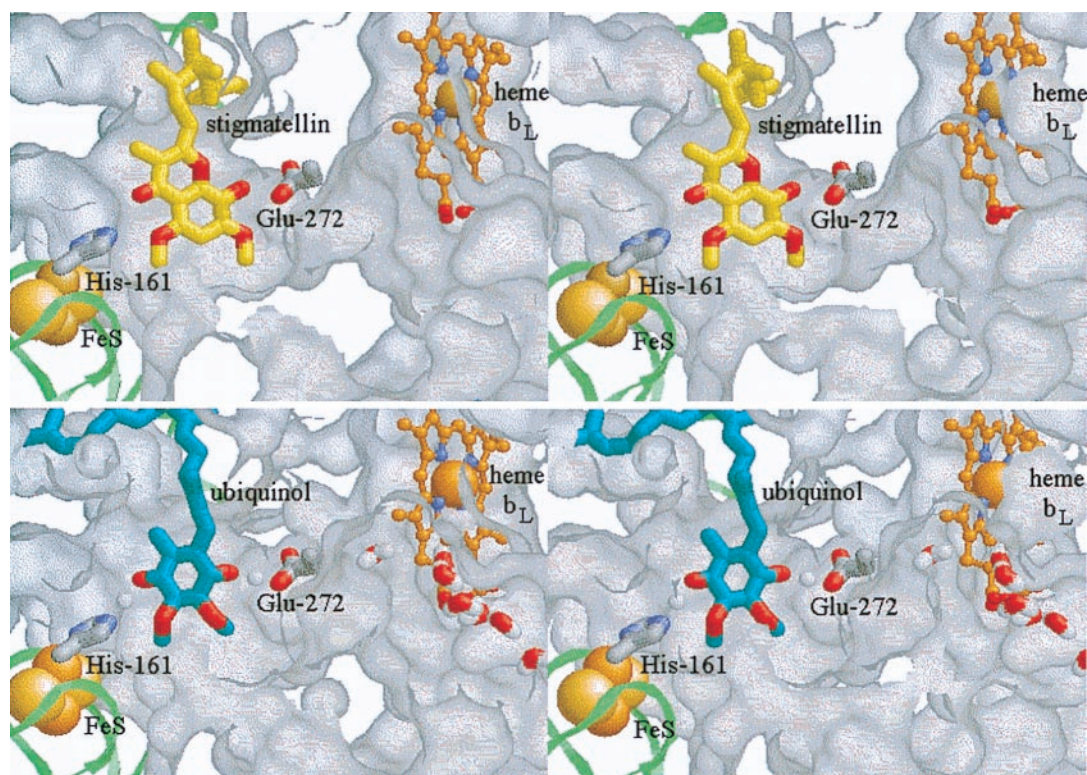
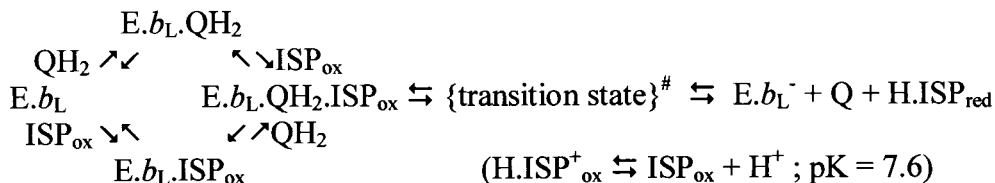


FIG. 1. Stigmatellin binding as a model for the enzyme–substrate complex. (Stereo pairs.) The ISP is shown as a pale green ribbon, with the 2Fe–2S cluster as space-filling spheres. *cyt b* is represented by the exterior surface of the protein, mapped with a 1.4-Å probe. The protein has been cut away to reveal the  $Q_o$ -site volume. The side chains of His-161 (ISP) and Glu-272 (*cyt b*) are shown as Corey–Pauling–Koltun (CPK) colored tube models, and heme  $b_L$  as a ball-and-stick model, with the Fe atom space-filling and C atoms in orange. (*Upper*) The binding of stigmatellin (C atoms yellow, O atoms red; from PDB 2bcc). (*Lower*) The enzyme–substrate complex: ubiquinol is shown with C atoms blue, O atoms red. A putative water chain (bottom right) occupies a channel in *cyt b* leading from the external aqueous phase to the heme  $b_L$  binding pocket and the  $Q_o$  pocket. See *Experimental Procedures* for model building and the text for discussion. These and the native and myxothiazol- and quinone-containing structures are available as supplementary material for interactive viewing through a Chime tutorial at [www.pnas.org](http://www.pnas.org).

ISP<sub>red</sub>. We have suggested that stigmatellin at the Q<sub>o</sub> site mimics the enzyme–substrate complex between quinol and ISP<sub>ox</sub> and shows the site of its formation (26, 27). In Fig. 1 *Lower*, we show a model of this reaction complex, in which quinol has been inserted into the stigmatellin structure in place of the inhibitor. The second reaction partner in formation of this complex is the mobile domain (head) of the ISP (8, 26, 27). We have suggested that movement of the head between interfaces on cyt *c*<sub>1</sub> and cyt *b* is essential for catalysis (8, 10, 26, 27). Because of this movement, the head of the ISP<sub>ox</sub> acts as a second substrate (*Scheme 1*).



SCHEME 1.

**Kinetic Assays of Substrate Binding.** The two binding processes can be distinguished by varying one or other substrate. Since other steps are not rate limiting, the rate of quinol oxidation can be measured by following the rate of reduction of either cyt *b*<sub>H</sub> (at pH <8.0) or cyt *b*<sub>L</sub> (at pH >8.5) in the presence of antimycin, which blocks electron transfer out of the cyt *b* chain (15–17). For the same reason, the rate can also be assayed in the absence of inhibitor by measuring the electrogenic processes associated with electron transfer through the *b*-cytochrome chain, through the electrochromic carotenoid change (6, 15, 28, 29). Using any of these approaches, we can vary [QH<sub>2</sub>] through redox titration at fixed pH. We can vary [ISP<sub>ox</sub>] separately by changing pH, while adjusting redox poise so as to keep the initial [QH<sub>2</sub>] constant (Fig. 2*A*). This latter approach depends on our suggestion that the species needed to bind in formation of the reaction complex is the dissociated ISP<sub>ox</sub> (19, 27).

For both substrates, the rate of quinol oxidation was dependent on substrate concentration. For changes in [QH<sub>2</sub>], we have previously shown that the rate saturates with the pool still partially oxidized, indicating a ≈30-fold tighter binding of QH<sub>2</sub> than Q (15, 17). The rate as a function of the calculated concentration of dissociated ISP<sub>ox</sub> ([ISP<sub>ox</sub>]) is shown in Fig. 2*B*, and it also shows a saturation curve. The curve is shifted so that the half-maximal rate occurs at pH ≈6.4, well below the pK at 7.6. From this, it seems likely that ISP<sub>ox</sub> is also preferentially bound in the reaction complex.

For neither substrate did the activation energy change with substrate concentration (Fig. 2*A*). We have previously shown that the activation energy was the same with the quinone pool either ≈50% reduced or initially oxidized (17). From the data it can be seen that the activation energy was the same whether the pool was 30% or 90% reduced, and whether the reaction was measured through reduction of heme *b*<sub>H</sub> or heme *b*<sub>L</sub>, or through the electrogenic reactions, and was independent of pH under all these conditions. In these experiments, because of the variation of *E*<sub>m</sub> of the quinone/quinol couple with pH or temperature, the *E*<sub>h</sub> at each pH was adjusted so that the initial concentration of quinol in any set was the same before flash activation. Since [ISP<sub>ox</sub>] varies with pH in the range below the pK, the lack of effect of pH on activation energy also shows that [ISP<sub>ox</sub>] did not effect the activation barrier (Fig. 2*A*). These results show that the step with a high activation energy was after formation of the enzyme–substrate complex, as previously noted by Crofts and Wang (17).

**Effects of Mutation.** Mutations at the residue equivalent to Glu-272 in the *Rb. sphaeroides* *bc*<sub>1</sub> complex (E295D, -G, and

-Q) show an inhibited rate of quinol oxidation (ref. 30 and see Table 1), and mutants at the equivalent residue in the *bc*<sub>6f</sub> complex (the related enzyme in oxygenic photosynthetic chains) are also inhibited (31). The E295G and E295Q mutants were most severely affected. The two more active strains (E295D and G) both showed resistance to stigmatellin (reported in ref. 3). This latter property is now explained by the liganding function identified here. Interactions between ISP and the occupant of the site have been studied through the change induced in the EPR spectrum of the 2Fe–2S center (21). We have suggested that this *g*<sub>r</sub> = 1.800 signal is diagnostic

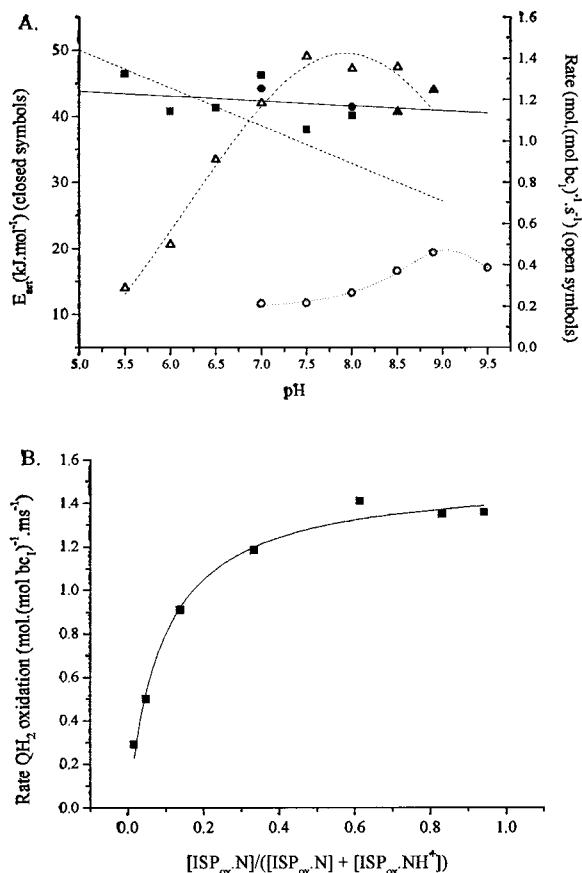


FIG. 2. Kinetic parameters for partial reactions. (A) Filled symbols (left-hand axis): Dependence of activation energy on pH for quinol oxidation. Each point represents a separate set of experiments in which the reaction was measured as a function of temperature and the data were analyzed with an Arrhenius plot. Reactions measured: ■, reduction of cyt *b*<sub>H</sub> (pH values <8.5), or ▲, reduction of cyt *b*<sub>L</sub> (pH values ≥8.5), with quinol pool 30% reduced; ●, slow phase of electrochromic change, with quinol pool 90% reduced. Solid line, linear fit to data; dashed line, slope of -5.7 kJ.mol<sup>-1</sup>. Open symbols (right-hand axis), rate of quinol oxidation: △, native *bc*<sub>1</sub> complex (average of two experiments, assayed by cyt *b*<sub>H</sub> reduction); ○, mutant Y156W (at 2 × scale, assayed through slow phase of electrochromic change, quinone pool 30% reduced). (B) The dependence of rate of quinol oxidation on concentration of ISP<sub>ox</sub>. Data from A for the pH dependence of cyt *b*<sub>H</sub> reduction have been replotted to show the variation of rate with dissociated [ISP<sub>ox</sub>], calculated using a pK of 7.6 on ISP<sub>ox</sub>.

Table 1. Mutations at Glu-295

Mutant*	$g_x^\dagger$ value	$g_x$ ampl.	Rate, $^\ddagger$ %	Relative $K_m^\S$	Inhibitor resist. $^\parallel$
Wild type	1.80	Large	100	1.0	None
E295D	—	—	11	1.54	Stig
E295G	1.80	Large	4.9	2.4	Stig
E295Q	1.81	Large	<4	—	—

\*Numbering from *Rb. sphaeroides* sequence; E295 is equivalent to E272 in chicken.

$^\dagger g_x$  value; band in the EPR spectrum of the ISP, centered at 1.80 in wild type, and associated with interaction between quinone and ISP<sub>red</sub>.

$^\ddagger$ Relative rate; the rate measured at  $E_h$  110 mV, normalized to the wild type and expressed as a percentage.

$^\S$ Relative  $K_m$ ; the  $K_m$  value determined from Lineweaver–Burke plots in which the concentration of QH<sub>2</sub> was estimated from the  $E_h$  and a value for  $E_{m,pH}$  of 90 mV. The molar concentration depends on the ratio  $Q_{tot}:bc_1$ , which is in the range 20–60, depending on assumptions. Assuming 30  $Q_{tot}:bc_1$ , and 1 mM  $bc_1$  in the membrane,  $K_m$  for wild type was 1.66 mM.

$^\parallel$ Inhibitor resistance; measured by titration of the amplitude of cyt *b* reduction in the presence of antimycin. Resistance to stigmatellin is indicated by Stig.

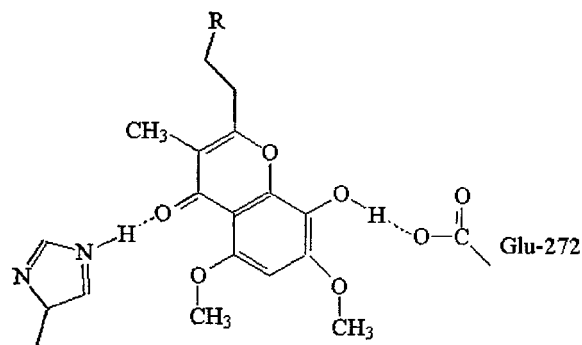
of complex formation between a single quinone occupant and the reduced subunit (26). In both E295G and E295Q strains, the  $g_x = 1.800$  signal appeared normal, showing that quinone could interact readily with ISP<sub>red</sub> despite the mutational change and the strongly inhibited electron transfer (Table 1). This finding suggests that although the glutamate is a ligand to stigmatellin (as seen in Fig. 1 *Upper*), it does not stabilize the binding of quinone. If Glu-272 provided a ligand to quinol, we might expect some effect on binding of substrate. In E295D the apparent  $K_m$  was marginally greater, but in E295G, it was substantially higher (2.4-fold) than wild type, in line with a weak liganding role (Table 1). The quinol oxidation in E295Q was so inhibited that no reliable  $K_m$  could be determined. On the basis of these effects, and the structural information, we propose that the ligation of stigmatellin, quinone, and quinol is as shown in Fig. 3.

## DISCUSSION

**Release of the First Proton.** Rich (32), from physicochemical studies of reactions between quinols and quinones in aqueous and aprotic media, suggested that oxidation of quinol must proceed through prior dissociation to the quinol anion, QH<sup>-</sup>. Because of the high pK of the first dissociation (pK >11.3), binding of quinol would likely be accompanied by a release of the first proton through stabilization by the protein. Brandt and colleagues (33, 34) have suggested an alternative model based on the observation that the activation energy measured in a steady-state assay showed a strong pH dependence, decreasing with increase in pH up to pH >9.5. This observation was interpreted as showing that dissociation of QH<sub>2</sub> to QH<sup>-</sup>, with the pK of the unbound quinol, was the process giving the high barrier.

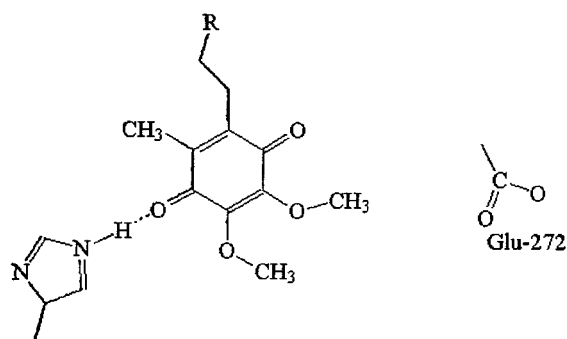
We have measured the pH dependence of the rates and activation energies of the kinetically accessible partial reactions of quinol oxidation (ref. 27, and see Fig. 2*A*), under conditions in which the initial concentrations of quinol and oxidant were the same (15–17, 27). In contrast to Brandt and Okun (33), we see no variation of activation energy for any of the partial reactions over the pH range 5.5 to 8.9. However, as with the mitochondrial complexes, we observed a strong dependence on pH of the rate of quinol oxidation (ref. 27 and Fig. 2). In our experiments this was measured under single-turnover conditions (6, 15), and analysis of the partial reactions showed that oxidation of quinol (rather than of the components of the high-potential chain) was the pH-dependent step.

### Liganding of stigmatellin



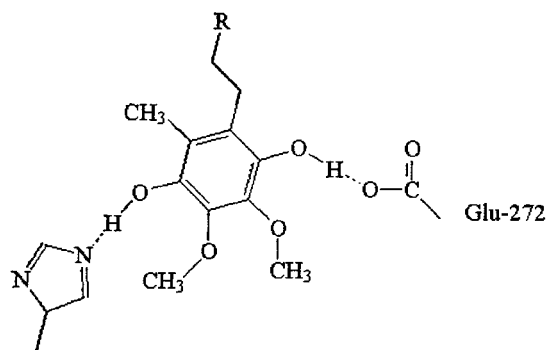
His-161 (ISP-red)

### Liganding of ubiquinone



His-161 (ISP-red)

### Liganding of ubiquinol



His-161 (ISP-ox)

FIG. 3. Liganding of  $Q_o$ -site occupants. Liganding of stigmatellin and quinone with ISP<sub>red</sub> and of quinol with ISP<sub>ox</sub>. Residues are numbered as in ref. 8.

This increase of rate with pH was observed only in the acidic range, up to pH  $\approx 7.5$  (27, 35). In view of the pK  $\approx 7.6$  on the oxidized ISP measured through redox titrations as a function of pH (19, 35), we suggested that this was a more likely candidate to account for the pH dependence than the dissociation of quinol suggested by Brandt and Okun (33), and we proposed that formation of the reaction complex must therefore require the dissociated form (19, 27). This provides a pathway for release of the first proton from quinol, as shown in the overall mechanism we propose for the  $Q_o$  site in Fig. 4. Release occurs through H transfer from quinol to ISP (Fig. 4*A*, process 1), followed by movement of ISP extrinsic domain to the cyt  $c_1$  reaction interface (process 2), and oxidation of

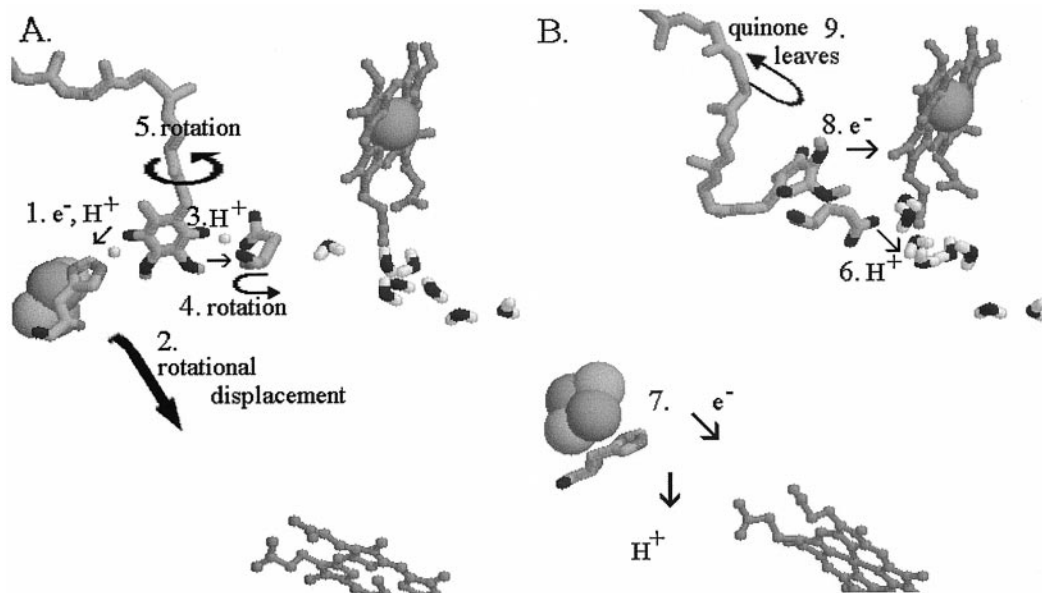


FIG. 4. Mechanism proposed for reactions at the Q<sub>o</sub> site after formation of the reaction complex. (A) The reaction complex between QH<sub>2</sub> bound in the distal domain and ISP<sup>ox</sup> bound at the interface on cyt *b*. The small white spheres show the H atoms of the H bonds, in both of which the quinol is the donor. The protein structure is that for the stigmatellin complex. (B) The reaction complex has dissociated to products, and the ISP<sup>red</sup> has moved to a position close to cyt *c*<sub>1</sub>. The protein structure is that for the myxothiazol complex. Numbers indicate the sequence of reactions. In the text, italic numbers refer to the numbered processes.

H·ISP<sup>red</sup> with release of H<sup>+</sup> (Fig. 4B, process 7). We recognize that the H-transfer process might be complex. The slow electron transfer ( $k \approx 1.5 \cdot 10^3 \text{ s}^{-1}$ ) over  $\approx 7 \text{ \AA}$  is of interest because the high activation barrier (45–65 kJ·mol<sup>-1</sup>) is likely in this step. The barrier could be contributed by any combination of the separate elements (electron transfer, H<sup>+</sup> transfer, and bond cleavage) involved. We will discuss the energy landscape of quinol oxidation in greater detail elsewhere (S.H., N.U., M.G.-K., and A.R.C., unpublished work). Snyder and Trumpower (36) have also briefly noted a possible role for dissociation of His-161 in proton processing.

To test this hypothesis, we have looked for mutant strains in which the pK on the ISP<sup>ox</sup> is modified. In a set of mutants constructed at Y165 (Y156 in *Rb. sphaeroides*), we have identified one strain, Y156W, in which the pK on ISP<sup>ox</sup> is shifted to higher pH (pK  $\approx 8.5$ ). The strain also showed a lowered midpoint potential ( $E_m \approx 198 \text{ mV}$ ) and a reduced rate of quinol oxidation. This mutant showed a shift in pH optimum for quinol oxidation to higher pH, as expected from our hypothesis (Fig. 2A). As in similar work with yeast *bc*<sub>1</sub> complex (37), the rate of quinol oxidation among mutant strains was dependent on the  $E_m$  value of the ISP. The decline in rate with decrease in  $E_m$ ,<sub>ISP</sub> supports the idea that the activation barrier is in this electron transfer step (17, 38).

**Release of the Second Proton.** The protein structures in Fig. 4 are those from the stigmatellin-containing (Fig. 4A) or myxothiazol-containing (Fig. 4B) crystals. In these models, the inhibitor has been replaced by quinol (Fig. 4A; see also Fig. 1 Lower), or quinone (Fig. 4B), constrained to the volume of the inhibitor-occupied site. As discussed above, it seems likely that stigmatellin might mimic the binding of both quinone (through the carbonyl H bond to His-161) and of quinol (through the hydroxyl H bond to Glu-272), as shown in Fig. 3. This possibility suggests a pathway for release of the second proton from the site. We propose that the H bond between Glu-272 and the stigmatellin -OH involves the dissociated glutamate and mimics a similar H bond formed on binding quinol. Release of the second proton would then involve H<sup>+</sup> transfer to Glu-272 to form the neutral acid (Fig. 4A, process 3), followed by rotation of the side chain (process 4), and release of the proton (Fig. 4B, process 6). Because, in the stigmatellin

structure, the Glu-272 side chain constricts the proximal domain of the Q<sub>o</sub> site (see Fig. 1 Upper), occupancy of this domain by inhibitor requires rotation of the side chain out of the site (process 4), as shown in Fig. 4B. If the semiquinone must move into the proximal domain before oxidation (process 5) as we have suggested (8, 26, 27), then rotation of the side chain would also have to occur before this could happen. We suggest that before rotation, the side chain must be protonated by dissociation of the neutral semiquinone to form the semiquinone anion, which would move to the proximal domain. The semiquinone anion would then be the species donating an electron to heme *b*<sub>L</sub> (process 8). Because movement of neither species includes a substantial vectorial displacement across the low-dielectric phase, the electrogenic contribution would be minimal, as seen experimentally (28). The structures show that rotation of the side chain to the “out” position brings the polar group to the surface of a channel into cyt *b* from the aqueous phase (process 6), which also connects to the heme *b*<sub>L</sub> propionates. It seems likely that this channel contains a water chain to facilitate transfer of the proton from Glu-272 to the exterior, as suggested in ref. 39 and shown by the waters modeled in Figs. 1 Lower and 4. Support for a role of Glu-272 in proton processing also comes from the work from Joliot’s lab on mutants in *Chlamydomonas* at the equivalent residue, which were modified in electron transfer, and in the kinetics of electrogenic events measured through the electrochromic response (31).

We thank Prof. P. L. Dutton and H. Ding for help with EPR spectroscopy of the Glu-295 mutants. We acknowledge with gratitude the support for this research provided by National Institutes of Health Grants GM 35438 (to A.R.C.) and DK 44842 (to E.A.B.) and by the Office of Health and Environmental Research, U.S. Department of Energy, under contract DE-AC03-76SF00098 (E.A.B.).

1. Cramer, W. A., Soriano, G. M., Ponomarev, M., Huang, D., Zhang, H., Martinez, S. E. & Smith, J. L. (1996) *Annu. Rev. Plant Physiol. Plant Mol. Biol.* **47**, 477–508.
2. Nitschke, W., Muehlenhoff, U. & Liebl, U. (1997) in *Photosynthesis: A Comprehensive Treatise*, ed. Raghavendra, A. (Cambridge Univ. Press, Cambridge, U.K.), pp. 285–304.

3. Brasseur, G., Sami Saribas, A. & Daldal, F. (1996) *Biochim. Biophys. Acta* **1275**, 61–69.
4. Degli Esposti, M., De Vries, S., Crimi, M., Ghelli, A., Patarnello, T. & Meyer, A. (1993) *Biochim. Biophys. Acta* **1143**, 243–271.
5. Brandt, U. & Trumpower, B. L. (1994) *CRC Crit. Rev. Biochem.* **29**, 165–197.
6. Crofts, A. R. & Wraight, C. A. (1983) *Biochim. Biophys. Acta* **726**, 149–186.
7. Xia, D., Yu, C.-A., Kim, H., Jia-Zhi Xia, J.-Z., Kachurin, A. M., Zhang, L., Yu, L. & Deisenhofer, J. (1997) *Science* **277**, 60–66.
8. Zhang, Z., Huang, L.-S., Shulmeister, V. M., Chi, Y.-I., Kim, K.-K., Hung, L.-W., Crofts, A. R., Berry, E. A. & Kim, S.-H. (1998) *Nature (London)* **392**, 677–684.
9. Iwata, S., Lee, J. W., Okada, K., Lee, J. K., Iwata, M., Rasmussen, B., Link, T. A., Ramaswamy, S. & Jap, B. K. (1998) *Science* **281**, 64–71.
10. Crofts, A. R. & Berry, E. A. (1998) *Curr. Opin. Struct. Biol.* **8**, 501–509.
11. Ljungdahl, P. O., Pennoyer, J. D., Robertson, D. E. & Trumpower, B. L. (1987) *Biochim. Biophys. Acta* **891**, 227–241.
12. Andrews, K. M., Crofts, A. R. & Gennis, R. B. (1990) *Biochemistry* **29**, 2645–2651.
13. Guergova-Kuras, M., Salcedo-Hernandez, R., Bechmann, G., Kuras, R., Gennis, R. B. & Crofts, A. R. (1998) *Protein Expression Purif.* **15**, 370–380.
14. Mitchell, P. (1976) *J. Theor. Biol.* **62**, 327–367.
15. Crofts, A. R., Meinhardt, S. W., Jones, K. R. & Snozzi, M. (1983) *Biochim. Biophys. Acta* **723**, 202–218.
16. Crofts, A. R. (1985) in *The Enzymes of Biological Membranes*, ed. Martonosi, A. N. (Plenum, New York), Vol. 4, pp. 347–382.
17. Crofts, A. R. & Wang, Z. (1989) *Photosynth. Res.* **22**, 69–87.
18. Surles, M., Richardson, J., Richardson, D. & Brooks, F. (1994) *Protein Sci.* **3**, 198–210.
19. Ugulava, N. & Crofts, A. R. (1998) *FEBS Lett.* **440**, 409–413.
20. Yun, C.-H., Wang, Z., Crofts, A. R. & Gennis, R. B. (1992) *J. Biol. Chem.* **267**, 5901–5909.
21. Ding, H., Robertson, D. E., Daldal, F. & Dutton, P. L. (1992) *Biochemistry* **31**, 3144–3158.
22. Iwata, S., Saynovits, M., Link, T. A. & Michel, H. (1996) *Structure* **4**, 567–579.
23. Kuila, D., Schoonover, J. R., Dyer, R. B., Batie, C. J., Ballou, D., Fee, J. A. & Woodruff, W. H. (1992) *Biochim. Biophys. Acta* **1140**, 175–183.
24. Lancaster, C. R. & Michel, H. (1997) *Structure* **5**, 1339–1359.
25. Link, T. A. (1997) *FEBS Lett.* **412**, 257–264.
26. Crofts, A. R., Barquera, B., Gennis, R. B., Kuras, R., Guergova-Kuras, M. & Berry, E. A. (1999) in *The Phototrophic Prokaryotes*, eds. Peschek, G. A., Loeffelhardt, W. & Schmetterer, G. (Plenum, New York), pp. 229–239.
27. Crofts, A. R., Berry, E. A., Kuras, R., Guergova-Kuras, M., Hong, S. & Ugulava, N. (1999) in *Photosynthesis: Mechanisms and Effects*, ed. Garab, G. (Kluwer, Dordrecht, The Netherlands), Vol. 3, pp. 1481–1486.
28. Glaser, E. G. & Crofts, A. R. (1984) *Biochim. Biophys. Acta* **766**, 322–333.
29. Venturoli, G., Fernandez-Velasco, J. G., Crofts, A. R. & Melandri, B. A. (1988) *Biochim. Biophys. Acta* **935**, 258–272.
30. Crofts, A. R., Barquera, B., Bechmann, G., Guergova, M., Salcedo-Hernandez, R., Hacker, B., Hong, S. & Gennis, R. B. (1995) in *Photosynthesis: From Light to Biosphere*, ed., Mathis, P. (Kluwer, Dordrecht, The Netherlands), Vol. 2, pp. 493–500.
31. Zito, F., Finazzi, G., Joliot, P. & Wollman, F.-A. (1998) *Biochemistry* **37**, 10395–10403.
32. Rich, P. R. (1981) *Biochim. Biophys. Acta* **637**, 28–33.
33. Brandt, U. & Okun, J. G. (1997) *Biochemistry* **36**, 11234–11240.
34. Brandt, U. (1998) *Biochim. Biophys. Acta* **1365**, 261–268.
35. Link, T. A. (1994) *Biochim. Biophys. Acta* **1185**, 81–84.
36. Snyder, C. & Trumpower, B. L. (1998) *Biochim. Biophys. Acta* **1365**, 125–134.
37. Denke, E., Merbitzshradnik, T., Hatzfeld, O. M., Snyder, C. H., Link, T. A. & Trumpower, B. L. (1998) *J. Biol. Chem.* **273**, 9085–9093.
38. Van Doren, S. R., Gennis, R. B., Barquera, B. & Crofts, A. R. (1993) *Biochemistry* **32**, 8083–8091.
39. Izrailev, S., Crofts, A. R., Berry, E. A. & Schulten, K. (1999) *Biophys. J.*, in press.